Bulletin of the Seismological Society of America, Vol. 84, No. 3, pp. 935–953, June 1994

Static Stress Changes and the Triggering of Earthquakes

by Geoffrey C. P. King, Ross S. Stein, and Jian Lin

Abstract To understand whether the 1992 $M = 7.4$ Landers earthquake changed the proximity to failure on the San Andreas fault system, we examine the general problem of how one earthquake might trigger another. The tendency of rocks to fail in a brittle manner is thought to be a function of both shear and confining stresses, commonly formulated as the Coulomb failure criterion. Here we explore how changes in Coulomb conditions associated with one or more earthquakes may trigger subsequent events. We first consider a Coulomb criterion appropriate for the production of aftershocks, where faults most likely to slip are those optimally orientated for failure as a result of the prevailing regional stress field and the stress change caused by the mainshock. We find that the distribution of aftershocks for the Landers earthquake, as well as for several other moderate events in its vicinity, can be explained by the Coulomb criterion as follows: aftershocks are abundant where the Coulomb stress on optimally orientated faults rose by more than one-half bar, and aftershocks are sparse where the Coulomb stress dropped by a similar amount. Further, we find that several moderate shocks raised the stress at the future Landers epicenter and along much of the Landers rupture zone by about a bar, advancing the Landers shock by 1 to 3 centuries. The Landers rupture, in turn, raised the stress at site of the future $M = 6.5$ Big Bear aftershock site by 3 bars. The Coulomb stress change on a specified fault is independent of regional stress but depends on the fault geometry, sense of slip, and the coefficient of friction. We use this method to resolve stress changes on the San Andreas and San Jacinto faults imposed by the Landers sequence. Together the Landers and Big Bear earthquakes raised the stress along the San Bernardino segment of the southern San Andreas fault by 2 to 6 bars, hastening the next great earthquake there by about a decade.

Introduction

It is generally agreed that the greatest earthquakes in California are associated with the San Andreas or closely related faults, and thus when the Landers earthquake struck within 25 km of the San Andreas a major question concerned its potential influence on San Andreas behavior. In particular, were stresses redistributed in such a way as to increase the likelihood of future San Andreas earthquakes? In this article we examine this question within the broad context of seeking to understand more generally the causal relations between earthquakes. Briefly, we ask under what conditions does one earthquake trigger another.

It has long been recognized that while each event produces a net reduction of regional stress, events also result in stress increases. With further tectonic loading it seems logical that such sites of stress rise should be the foci of future events and therefore such events should be readily predictable from preceding ones. Despite the apparent simplicity of this mechanical argument, earthquake triggering has not been observed as widely as might be expected. Phenomena such as the steady migration of epicenters along the North Anatolian (Ambraseys, 1970) and San Jacinto (Sanders, 1993) faults, for example, occur, but are rare.

Recent ideas of self-organized criticality (e.g., Bak and Tang, 1989; Cowie *et al.*, 1993) help to explain this result. If the Earth behaves in the way these authors suggest, all parts of the brittle crust are at the point of failure and, as a result of long-range elastic correlations, an earthquake can be followed by a nearby or a distant event. Thus, strong correlations between neighboring events need not dominate the physics of earthquakes. Nonetheless, in this article we show that local triggering effects can be clearly observed. We adopt classical concepts of stress transfer to explore interaction effects. The Coulomb failure stress changes caused by mainshock rupture effectively explain the aftershock distributions for the earthquakes we study, with some of the more distant events

apparently being triggered by stress changes of less than 1 bar. Not only do aftershocks appear to be triggered by such stress changes, but moderate events prior to the Landers earthquake increased the potential for failure along most of the future Landers rupture zone, perhaps controlling the location of the later rupture.

Associating co-seismic stress changes with earthquakes that take place days to years later is a substantial simplification of the physical process involved in earthquake triggering. Nonetheless, the spatial correlations that we find are compelling. We note that the time-dependent processes of deep fault creep and viscous relaxation of the asthenosphere will increase the static stress changes at seismogenic depths, but the spatial distribution of the Coulomb stress change will not greatly change.

These observations encourage us to apply stress interaction techniques to estimate how the potential for failure along parts of the San Andreas and associated faults has been changed by the Landers earthquake and, furthermore, to use these results to estimate the advance and delay of future large earthquakes on the San Andreas system.

Coulomb Failure

Various criteria have been used to characterize the conditions under which failure occurs in rocks. One of the more widely used is the Coulomb failure criterion, which requires that both the shear and normal stress on an incipient fault plane satisfy conditions analogous to those of friction on a preexisting surface. In the laboratory, confined rocks approximately obey the Coulomb failure conditions, which also appear to explain many field observations (Jaeger and Cook, 1979). Our approach is similar to those taken by Stein and Lisowski (1983), Oppenheimer *et al.* (1988), Hudnut *et al.* (1989), Reasenberg and Simpson (1992), Larsen *et al.* (1992), Harris and Simpson (1992), Jaumé and Sykes (1992), and Stein *et al.* (1992).

In the Coulomb criterion, failure occurs on a plane when the Coulomb stress σ_f exceeds a specific value

$$\sigma_f = \tau_\beta - \mu(\sigma_\beta - p), \tag{1}$$

where τ_β is the shear stress on the failure plane, σ_β is the normal stress, p is the pore fluid pressure, and μ the coefficient of friction. The value of τ_β must always be positive in this expression, whereas the usual processes of resolving stress onto a plane may give positive or negative values depending on whether the potential for slip is right or left lateral. The sign of τ_β must therefore be chosen appropriately.

If the failure plane is orientated at β to the σ_1 axis, we can express the stress components applied to it in terms of the principal stresses

$$\sigma_\beta = \frac{1}{2}(\sigma_1 + \sigma_3) - \frac{1}{2}(\sigma_1 - \sigma_3)\cos 2\beta \tag{2}$$

$$\tau_\beta = \frac{1}{2}(\sigma_1 - \sigma_3)\sin 2\beta, \tag{3}$$

where σ_1 is the greatest principal stress and σ_3 is the least principal stress. Equation (1) then becomes

$$\sigma_f = \frac{1}{2}(\sigma_1 - \sigma_3)(\sin 2\beta - \mu\cos 2\beta) - \frac{1}{2}\mu(\sigma_1 + \sigma_3) + \mu p \tag{4}$$

Differentiating equation (4) as a function of β, one finds that the maximum Coulomb stress σ_f^{max} occurs when

$$\tan 2\beta = 1/\mu \tag{5}$$

Pore fluid pressure modifies the effective normal stress across the failure plane, as shown in equation (1). When rock stress is changed more rapidly than fluid pressure can change through flow, p can be related to confining stress in the rock by Skemptons coefficient B, where B varies between 0 and 1. Equation (4) and subsequent expressions can therefore be rewritten on the assumption that σ_β represents the confining stress as well as the normal stress on the plane (e.g., Simpson and Reasenberg, 1994)

$$\sigma_f = \tau_\beta - \mu'\sigma_\beta, \tag{6}$$

where the effective coefficient of friction is defined by $\mu' = \mu(1 - B)$.

The failure condition is inherently two dimensional, with the intermediate stress σ_2 playing no part. Thus, all of the processes that we consider can be illustrated in two dimensions. To generalize the mathematics to three dimensions it is only necessary to determine the orientation of the plane of greatest and least principal stresses in the appropriate coordinate system and to apply the failure conditions in that plane.

Two-Dimensional Case: Change of Coulomb Stress on Faults of Specified Orientation

In a system where the x and y axes and fault displacements are horizontal, and fault planes are vertical

(containing the z direction), stress on a plane at an angle Ψ from the x axis (Fig. 1) is given by

$$\sigma_{11} = \sigma_{xx}\cos^2\psi + 2\sigma_{xy}\sin\psi\cos\psi + \sigma_{yy}\sin^2\psi$$

$$\sigma_{33} = \sigma_{xx}\sin^2\psi - 2\sigma_{xy}\sin\psi\cos\psi + \sigma_{yy}\cos^2\psi$$

$$\tau_{13} = \frac{1}{2}(\sigma_{yy} - \sigma_{xx})\sin 2\psi + \tau_{xy}\cos 2\psi. \quad (7)$$

We can now write the change of Coulomb stress for right-lateral σ_f^R and left-lateral σ_f^L motion on planes orientated at ψ with respect to the x axis in the following way:

$$\sigma_f^R = \tau_{13}^R + \mu'\sigma_{33} \quad (8)$$

$$\sigma_f^L = \tau_{13}^L + \mu'\sigma_{33}. \quad (9)$$

The sign of τ_{13} from equation (7) is unchanged for right-lateral slip (τ_{13}^R) in equation (8) and reverses in sign for left-lateral slip (τ_{13}^L) in equation (9).

Equation (9) is illustrated in Figure 2a. An elliptical slip distribution is imposed on a master fault in a uniform, stress-free, elastic half-space. The contributions of the shear and normal components to the failure condition, and the resulting Coulomb stresses, for infinitesimal faults parallel to the master fault, are shown in separate panels. Such a calculation represents the change of Coulomb stress on these planes resulting only from slip on the master fault. The calculation is appropriate to determine, for example, the effect of Landers on a nearby segment of the San Andreas fault. One need only know the relative location of the San Andreas and Landers faults, the slip on the Landers fault, and the sense of slip on the San Andreas to determine whether the San Andreas fault has been brought closer to, or further from, failure. Such calculations are independent of any knowledge of the prevailing regional stresses or any preexisting stress fields from other events. The signs in the calculation are chosen such that a positive Coulomb stress indicates a tendency for slip in the same right-lateral sense as the fault of interest. Negative Coulomb stresses indicate a reduction of this tendency. It is important to appreciate that because τ_{13} changes sign between equations (8) and (9), a negative Coulomb stress for right-lateral fault motion is not the same as a tendency for left-lateral slip.

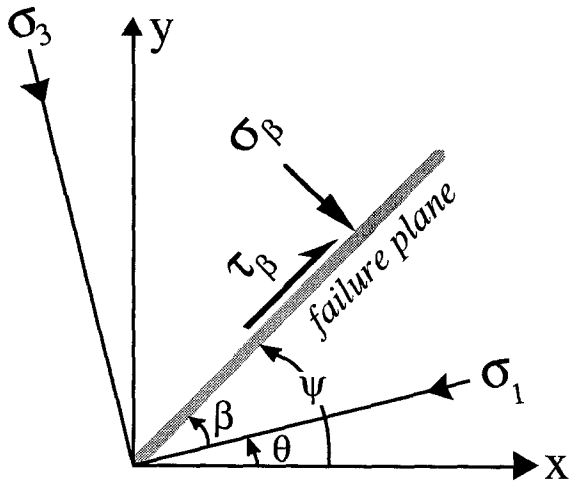

Figure 1. The axis system used for calculations of Coulomb stresses on optimum failure planes. Compression and right-lateral shear stress on the failure plane are taken as positive. The sign of τ_β is reversed for calculations of right-lateral Coulomb failure on specified failure planes.

The distribution of increases and decreases of Coulomb stress shows features common to all subsequent figures. Lobes of increased shear stress appear at the fault ends, corresponding to the stress concentrations that tend to extend the fault. Off-fault lobes also appear, separated from the fault by a region where the Coulomb stresses have not been increased, as discussed by Das and Scholz (1983). If the master fault were infinitesimal in length, the off-fault lobes would be equal in amplitude to the fault-end lobes at all distances. For a finite length fault they are absent near the fault and reduced in amplitude at moderate distances. The normal stress change field is similar to the more familiar dilatational field with maxima and minima distributed antisymmetrically across the fault, but here we consider only the component of tension normal to the fault. The influence of the normal stress on the Coulomb stress distribution is to reduce the symmetry of the final distribution and to increase the tendency for off-fault failure.

Two-Dimensional Case: Change of Coulomb Stress on Optimally Orientated Faults

Coulomb stress changes on optimally orientated planes can also be calculated as a result of slip on the master fault, and these are the planes on which aftershocks might be expected to occur. We presume that a sufficient number of small faults exist with all orientations and that the faults optimally orientated for failure will be most likely to slip in small earthquakes. After an earthquake, the optimum directions are determined not only by the stress change due to that earthquake σ_{ij}^q but also by pre-existing regional stresses σ_{ij}^r to give a total stress σ_{ij}^t

$$\sigma_{ij}^t = \sigma_{ij}^r + \sigma_{ij}^q. \quad (10)$$

The orientation of the principal axes resulting from the total stress are therefore derived using

$$\theta = \frac{1}{2}\tan^{-1}\left(\frac{2\sigma_{xy}^t}{\sigma_{xx}^t - \sigma_{yy}^t}\right). \quad (11)$$

Where θ is the orientation of one principal axis to the x

axis as shown in Figure 1 and the other is at $\theta \pm 90°$. From these two directions, the angle of greatest compression θ_1 must be chosen. Thus the optimum failure angle ψ_o is given by $\theta_1 \pm \beta$. Whereas the optimum planes are determined from σ'_{ij}, the normal and shear stress changes on these planes are determined only by the earthquake stress changes σ^q_{ij}. Thus the changes in stress on the optimum planes become

$$\sigma_{33} = \sigma^q_{xx} \sin^2\psi_o - 2\sigma^q_{xy} \sin\psi_o \cos\psi_o + \sigma^q_{yy} \cos^2\psi_o$$

$$\tau_{13} = \frac{1}{2}(\sigma^q_{yy} - \sigma^q_{xx}) \sin 2\psi_o + \tau^q_{xy} \cos 2\psi_o \qquad (12)$$

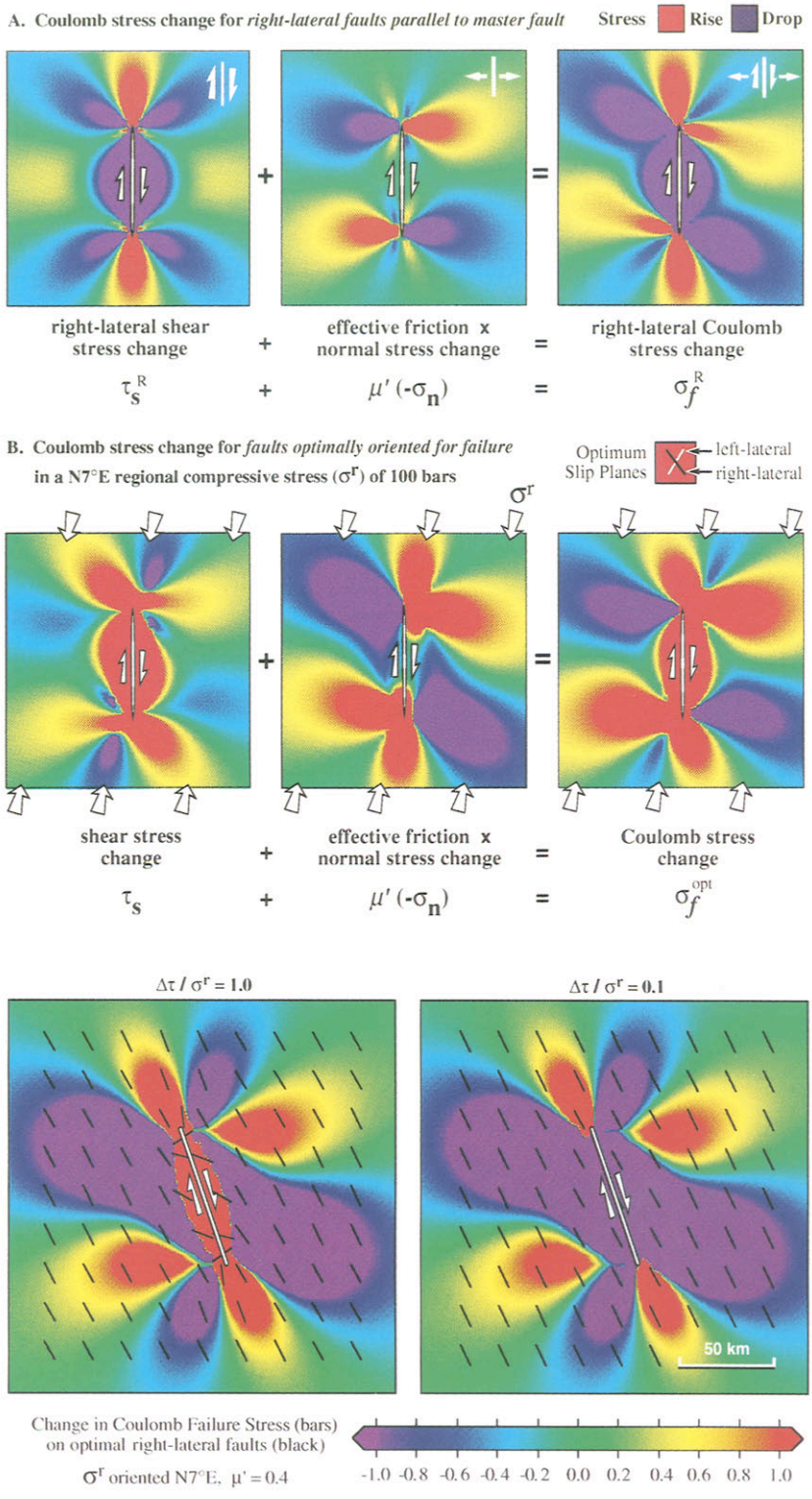

Figure 2. Illustration of the Coulomb stress change. The panels show a map view of a vertical strike-slip fault embedded in an elastic half-space, with imposed slip that tapers toward the fault ends. Stress changes are depicted by graded colors; green represents no change in stress. (a) Graphical presentation of equation (9). (b) Graphical presentation of equation (13).

Figure 3. Dependence of the Coulomb stress change on the regional stress magnitude. If the earthquake relieves all of the regional stress (*left panel*), resulting optimum slip planes rotate near the fault. If the regional deviatoric stress is much larger than the earthquake stress drop (*right panel*), the orientations of the optimum slip planes are more limited, and regions of increased Coulomb stress diminish in size and become more isolated from the master fault. In this and subsequent plots, the maximum and minimum stress changes exceed the plotted color bar range.

and the Coulomb stress changes

$$\sigma_f^{\text{opt}} = \tau_{13} - \mu'\sigma_{33}. \quad (13)$$

The two optimum planes correspond to left-lateral and right-lateral shear with expression (13) applying to both. It is important to emphasize that we calculate the change of Coulomb stress on planes that are optimum after the earthquake. The optimum orientations are calculated from the total stress after the earthquake, and the Coulomb stress changes caused by the earthquake stress changes are resolved onto these planes. In general, the earthquake rotates the principal axis. It is possible to calculate the change of maximum Coulomb stress at some point before and after the earthquake, together with the change of angle of the infinitesimal plane upon which it operates. However, we do not regard such effects as having significance for earthquake triggering.

The results of a calculation to find optimum orientations and magnitudes of Coulomb stress changes are shown in Figure 2b. The calculations are again in a half-space and the slip on the master fault is the same as before. A uniform 100-bar compressional stress is introduced with the orientation shown. White lines indicate optimum left-lateral orientations and black lines, right-lateral orientations. The shear and normal stress contributions to the Coulomb stress change are again shown in separate panels. It can be seen from expression (10) that only the deviatoric part of the regional stress determines the orientation of principal axes, and hence the optimum stress orientations. Thus, it is sufficient to apply the regional stress as a simple uniaxial compression or extension.

The relative amplitude of the regional stress σ^r to the earthquake stress drop $\Delta\tau$ might to be expected to have an effect. This is explored in Figure 3, which shows the Coulomb stress change σ_f^{opt} on optimally orientated right-lateral planes in which the regional field is equal to the stress drop $\Delta\tau$ (*left panel*) and 10 times $\Delta\tau$ (*right panel*). These examples span likely conditions. It is evident that, except close to the master fault, the orientations of the optimal planes and Coulomb stress changes on these planes are little altered. The optimal orientations are essentially fixed by the regional stress, except very close to the fault where the stress change caused by slip on the master fault is comparable to the regional stress. If the regional stress σ_{ij}^r were zero, then the Coulomb stress change on optimally oriented planes $\sigma_f^{\text{opt}} \geq \sigma_f^R$ or σ_f^L. If, however, the regional stress σ_{ij}^r is large relative to the earthquake stress drop, σ_f^R or σ_f^L may locally exceed σ_f^{opt}. In all calculations that follow, we use a uniform regional stress field σ_{ij}^r. However, this assumption is not required, and spatially variable stress fields can be incorporated into the calculation of σ_f^{opt}.

The effects of varying the orientation of regional stresses and changing the coefficient of friction μ' are shown in Figure 4. Possible changes of regional stress orientation are limited since the main fault must move as a result of the regional stress; the 30° range covers the likely range. Similarly, values of friction between 0.0 and 0.75 span the range of plausible values. All of the panels show the same general features, fault-end and off-fault Coulomb stress lobes. Thus, our modeling is most sensitive to the regional stress direction, modestly sensitive to the coefficient of effective friction, and insensitive to the regional stress amplitude.

Three-Dimensional Case: Strike-Slip and Dip-Slip Conditions

In the foregoing discussion we have assumed that only vertical faults are present and thus stress components σ_{zz}, σ_{xz}, and σ_{yz} could be neglected. In dip-slip faulting environments, however, these stress components cannot be ignored. If all of the regional stress components are known, one can calculate the orientation and magnitudes of the principal stresses. These can then used to calculate the orientation of the plane containing σ_1 and σ_3, and hence the optimum orientations of slip planes and the change of Coulomb failure stress on them can be found.

In practice this is not straightforward. While the vertical shear components of regional stress σ_{xz}^r and σ_{yz}^r can be ignored, the magnitude of the vertical stress σ_{zz}^r relative to the horizontal regional stresses σ_{yy}^r, σ_{xx}^r, and σ_{xy}^r cannot. The relative magnitude of the horizontal to vertical stresses determines whether events are strike slip or dip slip, and this can alter the form of the predicted Coulomb stress change distribution. Whereas in the two-dimensional case only the orientation of the regional stress is of consequence, for the three-dimensional case the ratio of the vertical to horizontal stresses becomes important, since this determines whether strike-slip or dip-slip faulting occurs. Direct information on relative stress amplitudes is not generally available and varies with depth, so alternative strategies must be adopted. One possibility is to select relative stresses such that the calculations predict the earthquake mechanisms observed. The second is determine probable fault orientations *a priori* and directly determine the Coulomb changes on them. Since focal mechanisms are the best guide to relative stresses and fault orientations, these two possibilities are different technically, but not in practice. Finally, where two principal stresses are nearly the same, the distributions of Coulomb stress changes for dip-slip and strike-slip faulting are similar.

Coulomb Stress Changes and Aftershocks

The methods outlined above can be applied to the aftershock distributions of two events that preceded the Landers event, the 1979 Homestead Valley sequence and the 1992 Joshua Tree earthquake (Figs. 5 and 6). Neither

event produced surface rupture directly attributable to the mainshock, but seismic and geodetic observations furnish evidence for the geometry of fault slip. The calculations are carried out in a half-space with the values of Coulomb stress plotted in the figures being calculated at half the depth to which the faults extend.

Both Figures 5 and 6 show the four characteristic lobes of increased Coulomb stress rise and four lobes of Coulomb stress drop. The lobes at the ends of the fault extend into the fault zone, while the off-fault lobes are separated from the fault over most of its length by a zone where the Coulomb stress is reduced. The distributions of aftershocks are consistent with these patterns. Increases of Coulomb stress of less than 1 bar appear to be sufficient to trigger events, while reductions of the same amount effectively suppress them. Relatively few events fall in the regions of lowered Coulomb stress, and the clusters of off-fault aftershocks are separated from the fault itself by a region of diminished activity. The distributions of Coulomb stresses can be modified as described earlier by adjusting the regional stress direction and changing μ'. However, any improvements in the correlation between stress changes and aftershock occurrence are modest. Consequently, we have chosen to show examples with an average μ' of 0.4. Whatever values we adopt, we find that the best correlations of Coulomb stress change to aftershock distribution are at distances greater than a few kilometers from the fault. Closer to the fault, unknown details of fault geometry and slip distribution influence stress changes. At distances larger than about three fault lengths, the correlations are less clear because there are fewer aftershocks.

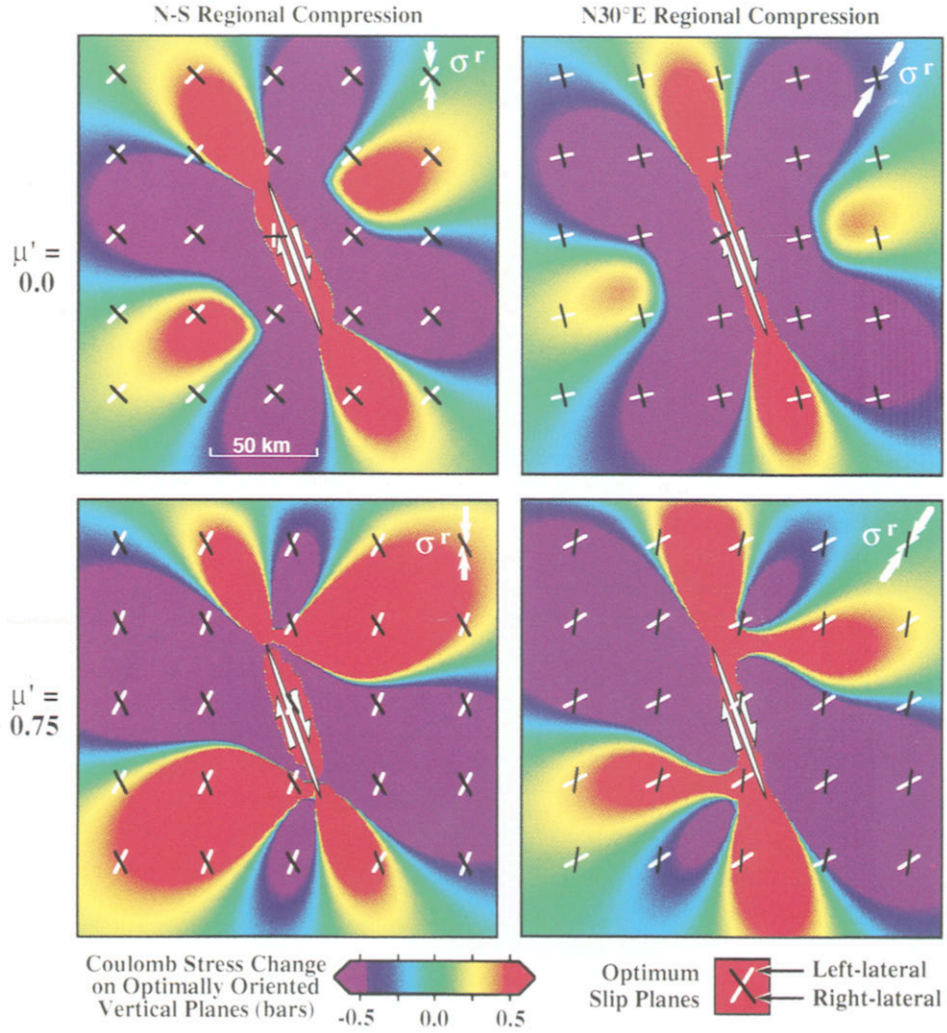

Figure 4. The effect of changing the regional stress σ^r orientation (*compare right and left panels*) and the effective coefficient of friction μ' (*compare top and bottom panels*). The example is for a simplified Landers rupture (5 m of tapered slip on a 70-km-long, 12.5-km-deep fault). Regional stress magnitude is 100 bars. Friction controls the internal angle between right- and left-lateral slip planes, and the influence of the normal stress change on failure. The regional stress orientation controls the size of off-fault to fault-end lobes.

An examination of the distribution of Coulomb stress changes with depth is also instructive. Figure 7 shows a cross section perpendicular to the Homestead Valley fault ($L/W \sim 1$). Increased Coulomb stresses can be seen in the off-fault lobes and at the base of the fault. Because the stress concentration beneath the fault lies at the depth at which stress is accommodated aseismically, this is typically free from aftershocks. The off-fault lobes, however, are seen in the well-located hypocentral distributions of the Homestead Valley (Hutton *et al.*, 1980; Stein and Lisowski, 1983). The predicted Coulomb stress increases diminish with depth away from the fault (Fig. 7), a feature that is also seen in the off-fault aftershock distributions, which extend to 60 to 80% of the depth of the mainshock and its deepest associated aftershocks. A similar accord between the Coulomb stress changes at depth and well-located aftershocks is seen for the Joshua Tree earthquake (Hauksson *et al.*, 1993).

Although events such as Homestead Valley and Joshua Tree have readily identifiable off-fault aftershock clusters, such features have not been observed on a large scale for great earthquakes on transcurrent faults with rupture lengths of many tens or even hundreds of kilometers. Scholz (1982) pointed out that fault slip scales differently for faults that are much longer than the thickness of the brittle crust. In Figure 8, stress changes caused by 1 of slip on a short fault (*left panel*) and a long fault (*right panel*) are compared. The lobes at the fault ends are similar in strength and size. For the short fault, the

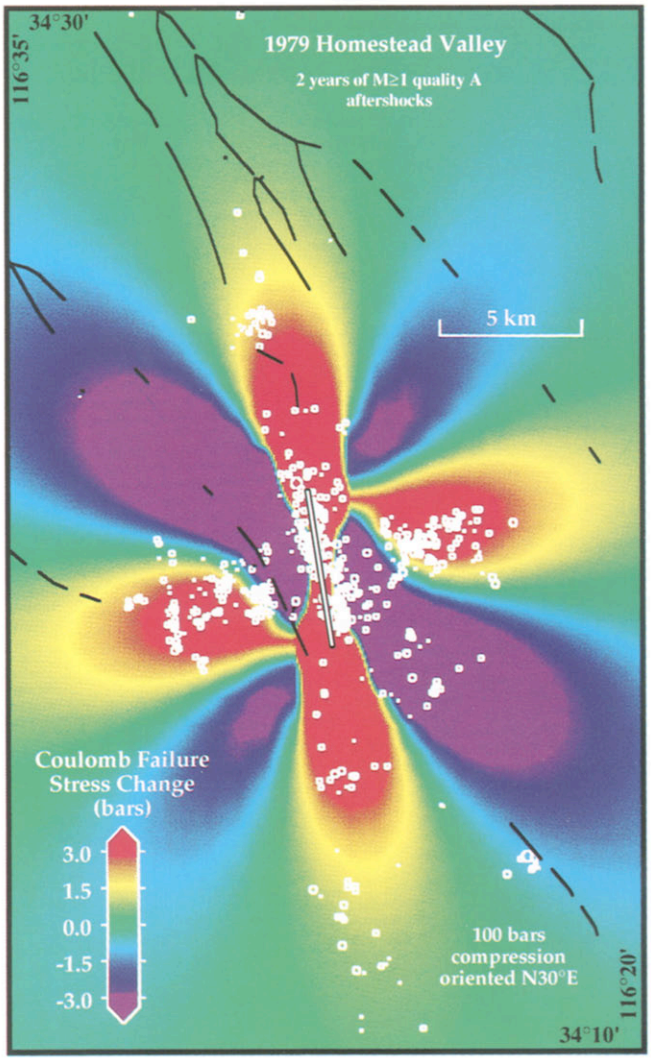

Figure 5. Coulomb stress changes associated with the 15 March 1979 Homestead Valley earthquake sequence (M_L = 4.9, 5.2, 4.5, and 4.8). The fault (enclosed white line) is 5.5-km long by 6-km deep, with 0.5 m of tapered slip and a moment of 4.2×10^{24} dyne-cm, following Stein and Lisowski (1983) and King *et al.* (1988). Stress is sampled halfway down the fault.

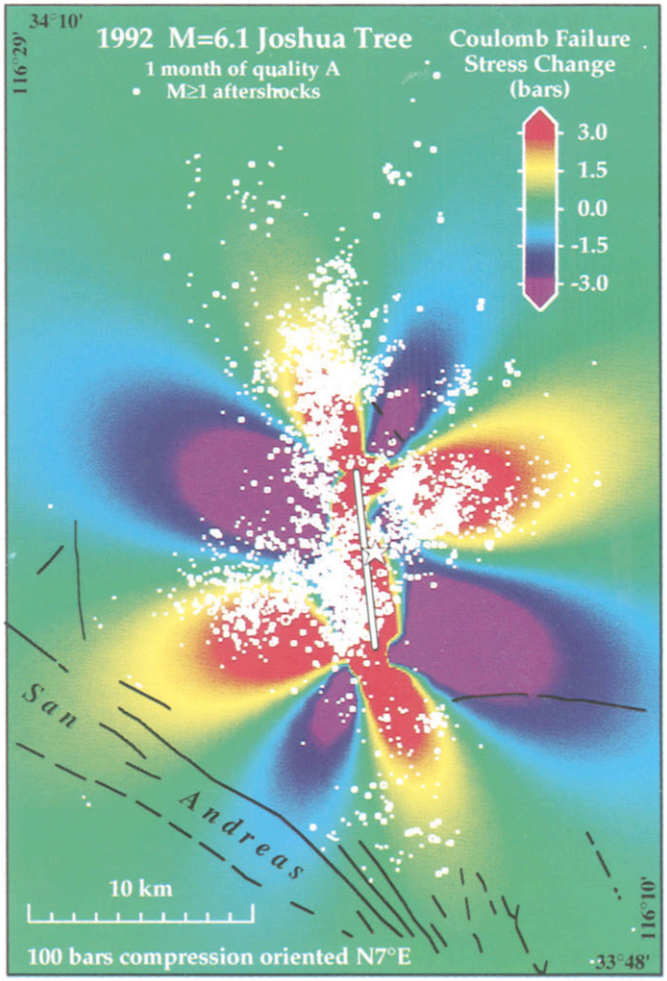

Figure 6. Coulomb stress changes calculated for the 23 April 1992 M_L = 6.1 Joshua Tree earthquake. The mainshock is indicated by the star. The model fault is 8-km long and 12.5-km deep with 0.5 m of right-lateral slip, for a moment of 2×10^{25} dyne-cm, following Savage *et al.* (1993) and Ammon *et al.* (1993). Stress is sampled halfway down the fault.

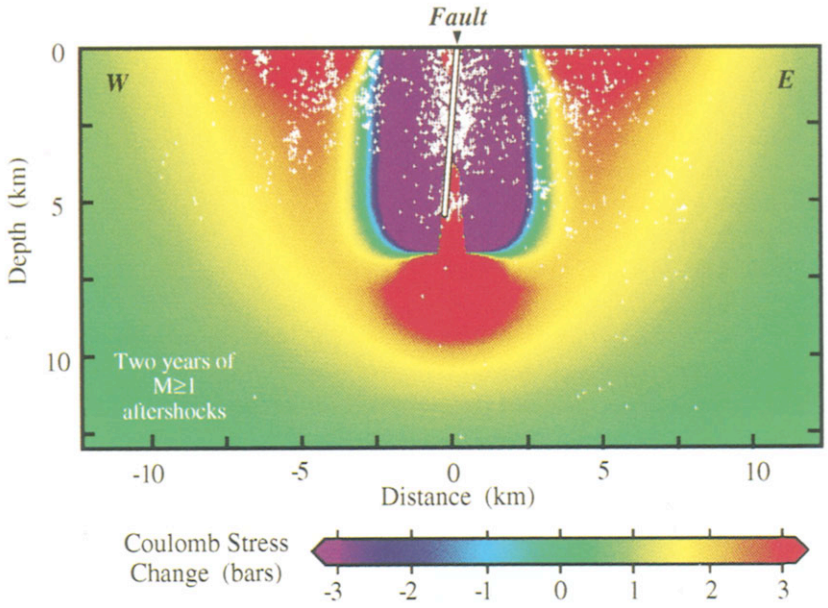

Figure 7. A depth cross section of Coulomb stress changes for the 1979 Homestead Valley fault (essentially the $L/W = 1$ fault in Fig. 8 made along the distance = 0 km line), with aftershocks from Hutton *et al.* (1980). Because the section does not pass through the centers of the off-fault lobes, the lobes appear shallower and smaller than at their maxima. The stress concentration at base of fault is exaggerated because fault slip is not tapered with depth.

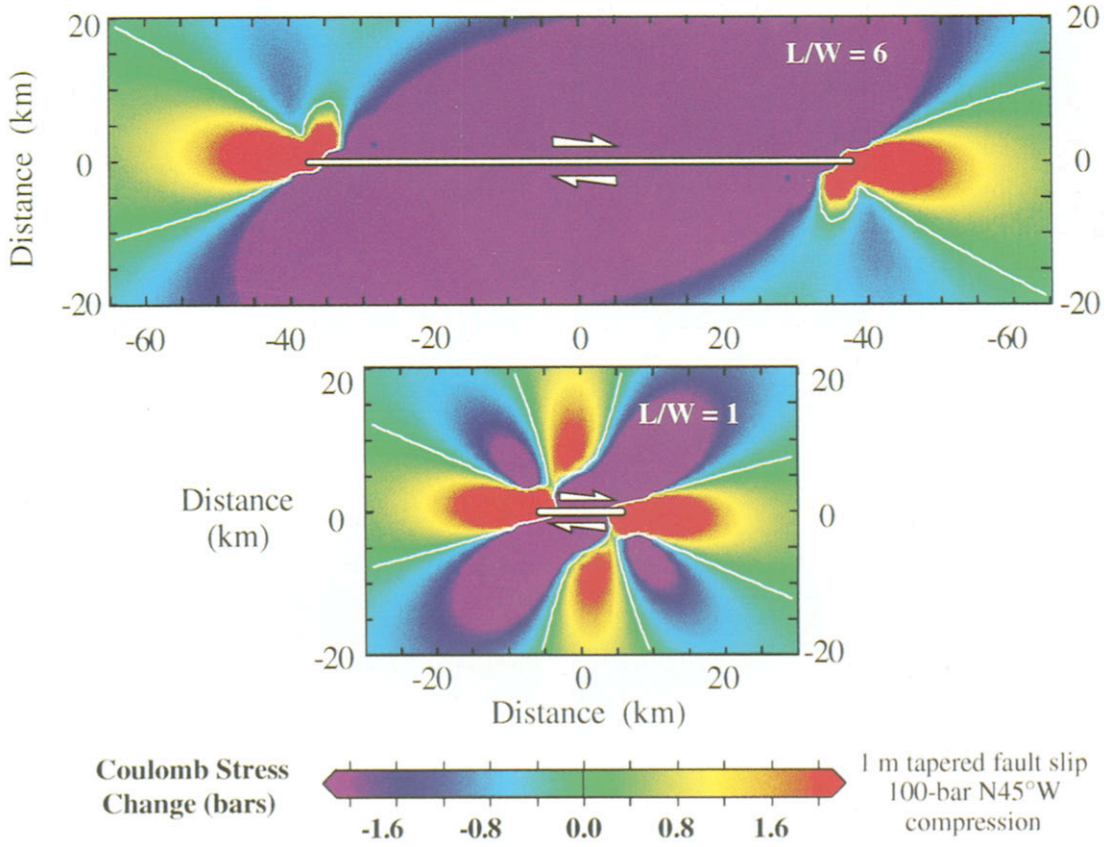

Figure 8. Coulomb stress changes as a function of fault length, L. Off-fault stress lobes diminish as the fault lengthens relative to its down-dip dimension, W. Both faults are 12.5-km deep with a stress drop of ~45 bars. Stress is sampled halfway down the fault.

off-fault lobes can be seen at distances from the fault of the order of one fault length, again with comparable strength. For the long faults the off-fault lobes have essentially disappeared.

Stress Changes Associated with the Landers Earthquake

Regional Stress Field Driving Rupture

For all subsequent calculations, we take the regional stress to be a simple compression of 100 bars, orientated at N7°E. As we demonstrate earlier, only the deviatoric part of the stress tensor is important and the amplitude hardly matters, provided that we can assume primarily strike-slip mechanisms, a reasonable assumption for the Landers region. Figure 4 shows that Coulomb stress changes are modestly sensitive to the orientation of the principal axes, and hence our choice of N7°E needs to be justified.

The principal strain axes can be used as an indication of stress orientation, with the direction of maximum shortening being taken to be the same as the axis of maximum compressive stress. Using geodetic data, Lisowski *et al.* (1991) found maximum shortening orientated at N7 ± 1°E during the pre-earthquake period 1979 to 1991 for the Joshua geodetic network, which includes most of the Landers rupture. They also found the same direction during the period 1934 to 1991 for the Landers and southern San Andreas regions. Across the north half of the Landers rupture, Sauber *et al.* (1986) found maximum shortening between 1934 and 1982 to lie at N4 ± 5°E. These values are all close to the maximum shortening axis predicted for simple shear between the Pacific and North America plates N9°E, given a relative plate motion direction in central California of N36°W (DeMets *et al.*, 1990).

Seismic focal mechanisms also supply information on the principal stress. The mean principal stress direction derived from small shocks along the 50 to 150 km of the San Andreas fault nearest to the Landers region (Banning and Indio segments) is N6 ± 2°E (Jones, 1988). Williams *et al.* (1990) found that the average principal stress direction for the 50-km stretch of the San Andreas fault adjacent to Landers (San Gregorio Pass and Eastern Transverse Range-I regions) to be N8 ± 5°E. Thus, several independent techniques yield a stress direction within a few degrees of our adopted value. Only data from the borehole at Cajon Pass (Zoback and Lachenbruch, 1992) gives a different orientation (N57 ± 19°E), but this could not drive local or regional right-lateral motion on the San Andreas fault and may instead be attributable to local effects (Shamir and Zoback, 1992).

Coulomb Stress Changes Preceding the Landers Rupture

In Figure 9 we show the Coulomb stress changes caused by the four $M > 5$ earthquakes within 50 km of

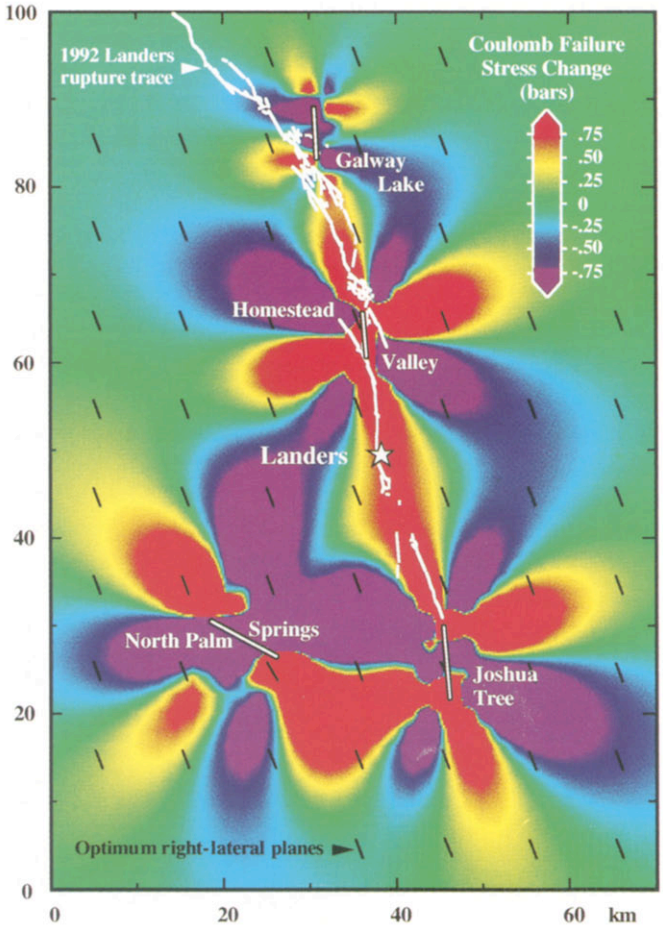

Figure 9. Coulomb stress changes calculated for the four $M > 5$ earthquakes in the Caltech-USGS catalog within 50 km of the future Landers epicenter. Each earthquake raised the stress at the future Landers epicenter (star). All ruptures (enclosed white lines) except the North Palm Springs shock are modeled as vertical right-lateral ruptures. The $M_L = 5.2$ Galway Lake earthquake is modeled with 0.07 m of slip on a 6-km-long fault, for a moment of 6.3×10^{23} dyne-cm (Hill and Beeby, 1977; Lindh *et al.*, 1978). The North Palm Springs fault dips 45° NE and has 0.42 m of right-lateral and 0.27 m of reverse slip, following Jones *et al.*, (1986), Pacheco and Nábelek (1988), and Savage *et al.* (1993).

Landers that preceded the Landers earthquake. The 1975 $M_L = 5.2$ Galway Lake, 1979 $M_L = 5.2$ Homestead Valley, 1986 $M_L = 6$ North Palm Springs, and 1992 $M_L = 6.1$ Joshua Tree earthquakes progressively increased Coulomb stresses by about 1 bar at the future Landers epicenter. Together they also produced a narrow zone of Coulomb stress increase of 0.7 to 1 bars, which the future 70-km-long Landers rupture followed for 70% of its length. The Landers fault is also nearly optimally oriented for failure along most of its length. The four moderate earthquakes may themselves have been part of a larger process of earthquake preparation within the

earthquake cycle, as suggested by Nur *et al.* (1993). It is noteworthy that the three largest events are roughly equidistant from the future Landers epicenter; the right-lateral Homestead Valley and Joshua Tree events enhanced stress as a result of the lobes beyond the ends of their ruptures, whereas the North Palm Springs event enhanced rupture as a result of an off-fault lobe. Increasing the effective friction from μ' from 0.4 (Fig. 9) to 0.75 slightly enhances the effects, and dropping the friction to zero reduces them.

Paleoseismic trench excavations across the Landers rupture suggest that the 1992 Landers fault last slipped about 6000 to 9000 yr ago (Hecker *et al.*, 1993; Rockwell *et al.*, 1993; Rubin and Sieh, 1993). The mean static stress drop of the 1992 Landers earthquake was about 35 bars, using a shear modulus of 3.3×10^{11} dyne-cm, and mean fault slip of 2.6 m and a fault width of 15 km from Wald and Heaton (1994). Thus, the 1-bar stress rise contributed by the neighboring earthquakes may represent about 150 to 250 yr of typical stress accumulation. The four moderate earthquakes can therefore be thought of as advancing the occurrence of the Landers earthquake by 1 to 3 centuries.

Rupture Model for the Landers Earthquake

Unlike the earthquake sources modeled so far, which we approximated by tapered slip on single planes, there is vastly more information about the $M = 7.4$ Landers source. Here we use Wald and Heaton's (1994) model of fault slip, which they derive from joint inversion of broadband teleseismic waveforms, near-field and regional strong motions, geodetic displacements from Murray *et al.* (1993), and surface fault slip measurements from Sieh *et al.* (1993). We smooth their 2 by 2 km variable slip model to 5 by 5 km, and retain their three planar fault segments (Fig. 10). Cohee and Beroza (1994) found a similar slip distribution from near-source low-gain seismograms. Using a shear modulus of 3.3×10^{11} dyne-cm^{-2}, in the range typically employed to derive seismic moment, this slip distribution gives a total Landers seismic moment of 0.9×10^{27} dyne-cm

Stress Changes following the Landers Rupture but before the Big Bear Earthquake

The stress changes caused by the Landers event are shown in Figure 11. At first glance the off-fault stress lobe to the west of the fault appears surprisingly large, considering the 70-km length of the surface rupture. Inspection of Figure 10 reveals, however, that most of the fault slip is confined to a 40-km-long, 15-km-deep central section. Thus, the source has an effective L/W ratio of 2 to 3, rather than 6, as it would appear from the length of the surface rupture, which results in large off-fault lobes (Fig. 8). The western off-fault lobe is large at the expense of the eastern lobe because of the fault curvature, with the off-fault stresses adding on the concave side of the fault. These two factors account for the concentration of stress 20 km west of the Landers rupture, where the Big Bear aftershock would occur.

The largest lobe of increased Coulomb stress is centered on the epicenter of the future $M_L = 6.5$ Big Bear event, where stresses were raised 2 to 3 bars. The Big Bear earthquake was apparently initiated by this stress rise 3 hr 26 min after the Landers mainshock. The Coulomb stress change at the epicentre is greatest for high effective friction but remains more than 1.5 bars for $\mu = 0$. There is no surface rupture or Quaternary fault trace associated with the Big Bear earthquake. Judging from its epicenter and focal mechanism, Hauksson *et al.* (1993) suggest left-lateral rupture on the plane that is seen to be optimally aligned for failure, with the rupture apparently propagating northeast and terminating where the Landers stress change became negative. Jones and Hough (1994), however, argue for a multiple event with both right- and left-lateral rupture on orthogonal faults bisecting at the epicenter. In this case as well, rupture on each plane terminates where the stress changes become negative.

In addition to calculating the stress changes caused by the Landers rupture, we estimate the slip on the Big Bear fault needed to relieve the shear stress imposed by the Landers rupture. This is achieved by introducing a freely slipping boundary element along the future Big Bear rupture. The potential-slip along the Big Bear fault is 60 mm (left lateral), about 5 to 10% of the slip that occurred several hours later. These calculations suggest that the Big Bear slip needed to relieve the stress imposed by Landers was a significant fraction of the total slip that later occurred. Thus, from consideration of the stress changes and the kinematic response to those changes, it is reasonable to propose that stresses from the Landers event played a major role in triggering the Big Bear shock.

Stress Changes Caused by the Landers, Big Bear, and Joshua Tree Ruptures

The Big Bear earthquake was the largest of more than 20,000 aftershocks located after the Landers earthquake, large enough to result in significant stress redistribution at the southwestern part of the Landers rupture zone. Consequently, the distribution of later events cannot be examined without considering its effect. Although smaller, a similar argument can be applied to the Joshua Tree event, whose aftershock sequence was not complete at the time of the Landers rupture. In Figure 12 we therefore plot the combined Coulomb stress changes for the Joshua Tree, Landers, and Big Bear earthquakes. This distribution is shown together with all well-located $M_L \geq 1$ earthquakes that occurred in the box shown, within

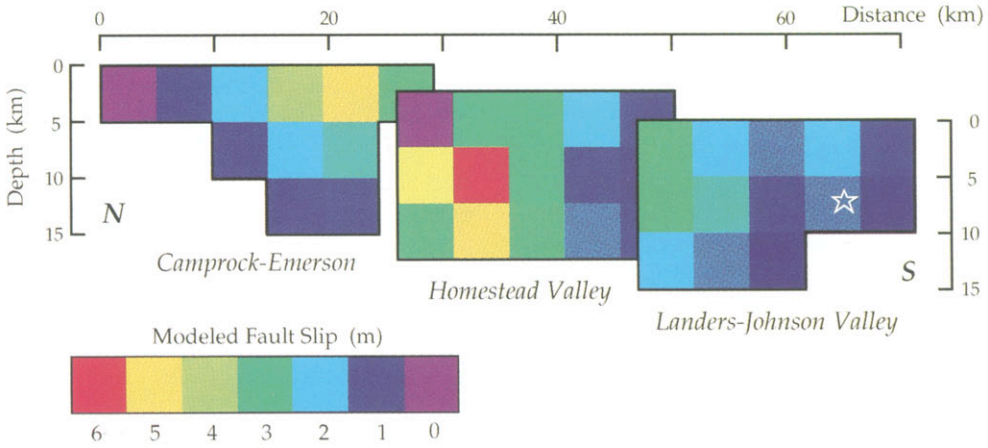

Figure 10. Distribution of modeled fault slip for the Landers earthquake from Wald and Heaton (1994), derived from joint inversion of strong motion, teleseismic, geodetic, and surface slip data. Three planar fault segments are used, which correspond approximately to the mapped fault trace. Although the surface rupture is 70-km long, the fault slip is concentrated over a strike length of just 40 km.

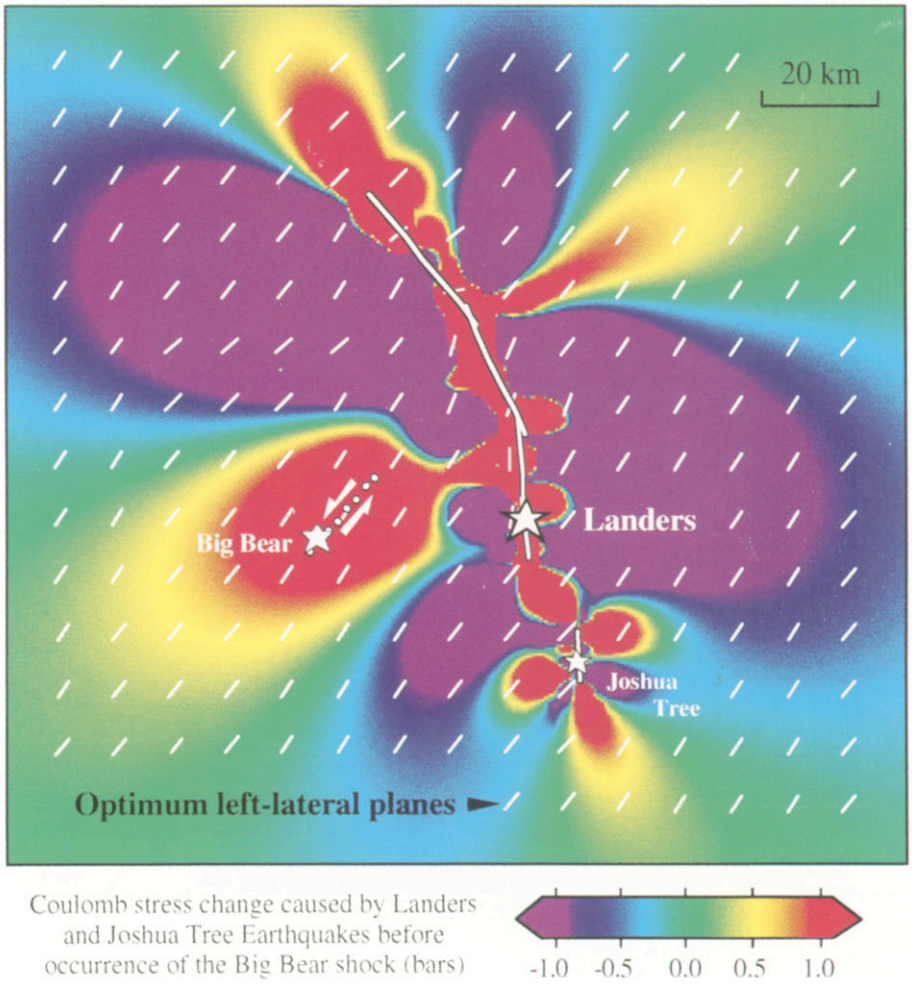

Figure 11. Coulomb stress change caused by the Landers rupture. The left-lateral M_L = 6.5 Big Bear rupture occurred along dotted line 3 hr 26 min after the Landers mainshock. The Coulomb stress increase at the future Big Bear epicenter is 2.2 to 2.9 bars.

about 250 km of the 28 June mainshock, during the following 25 days.

Most $M_L > 1$ aftershocks occur in regions where the failure stress is calculated to have increased by ≥ 0.1 bar, and few events are found where the stress is predicted to have dropped (Fig. 12). Even when all seismicity within 5 km of the Landers, Big Bear, and Joshua Tree faults is excluded, more than 75% of the aftershocks occur where the stress is predicted to have risen by >0.3 bar. In contrast, less than 25% of the aftershocks occur where the stress dropped by >0.3 bar. The same correspondence can be found among $M_L \geq 4$ earthquakes that took place during the 9-month period April through December 1992 from Hauksson *et al.* (1993). The largest shock to fall on or near the San Andreas, the 29 June 1992 $M_L = 4.7$ Yucaipa event (due east of San Bernardino in Fig. 13), occurred where the failure stress change on the San Andreas is calculated to have risen by 5 bars. Aftershocks to Landers also occurred as far as 1250 km north of the mainshock, largely in geothermal areas (Hill *et al.*, 1993). At these distances, the static Coulomb stress changes are much smaller than the tidal

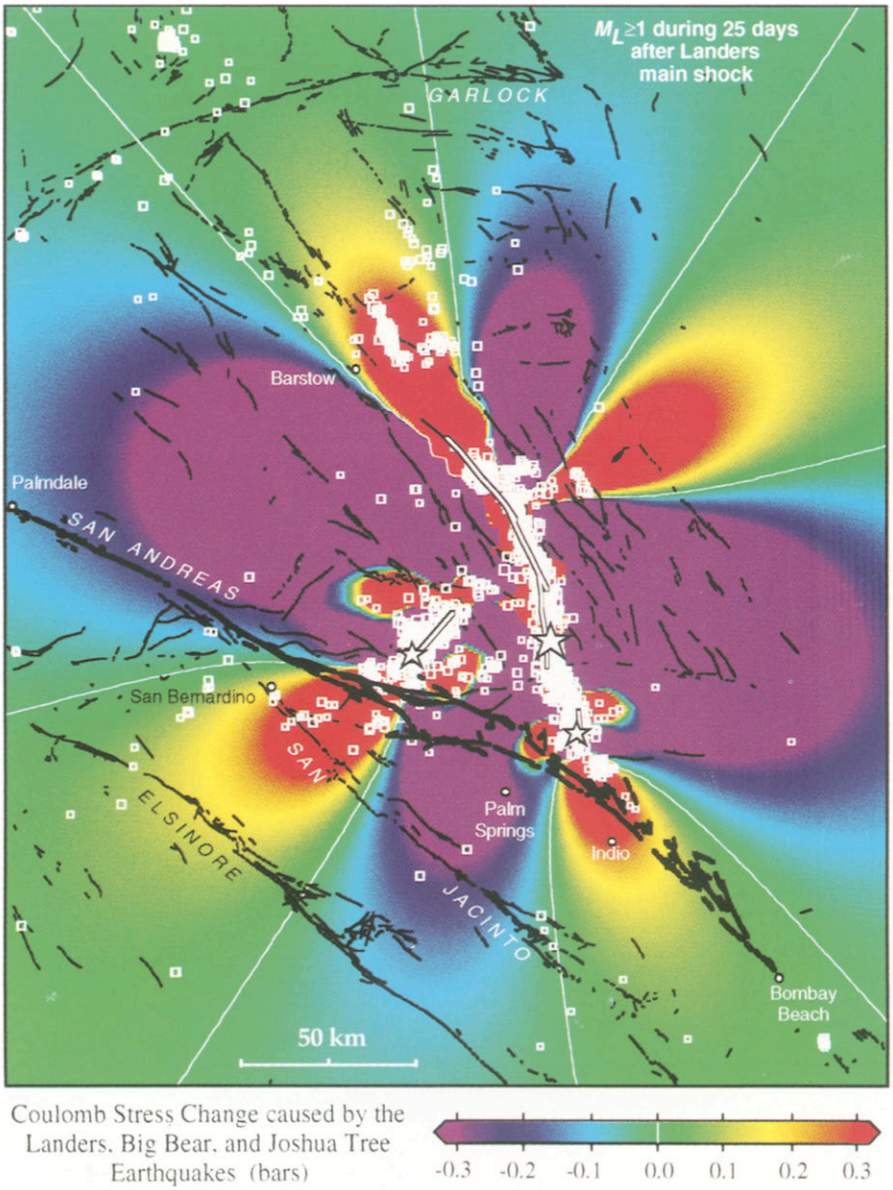

Figure 12. Coulomb stress changes at a depth of 6.25 km caused by the Landers, Big Bear, and Joshua Tree earthquakes. The Big Bear earthquake, which lacked surface rupture, is modeled as an 18-km-long by 12.5-km-deep vertical fault with 0.83 m of left-lateral slip, for a moment of 5.5×10^{25} dyne-cm, following limited seismic (Hauksson *et al.*, 1993) and geodetic (Murray *et al.*, 1993; Massonnet *et al.*, 1993) evidence.

stress changes, and thus we do not attempt to include them in our modeling.

Few aftershocks are seen near Indio in the Coachella Valley where the San Andreas was loaded by the Landers earthquake and, to a lesser extent, by the Imperial Valley (Hanks and Allen, 1989), Elmore Ranch, and Superstition Hills (Hudnut *et al.*, 1989) events [the effect of these earthquakes is shown in Stein *et al.* (1992)]. The lack of earthquakes near Indio appears to be an exception to the observation that Coulomb stress rises are accompanied by at least some activity, although triggered surface slip was seen at several points between Indio and the southeastern end of the San Andreas (D. Ponti, personal comm., 1992). Landers aftershocks could be absent in the Coachella Valley because the total stress there is lower, because the fault is locally tougher, or because modulus contrasts modify the Coulomb stresses. We examined the effect of a low-modulus Mojave tec-

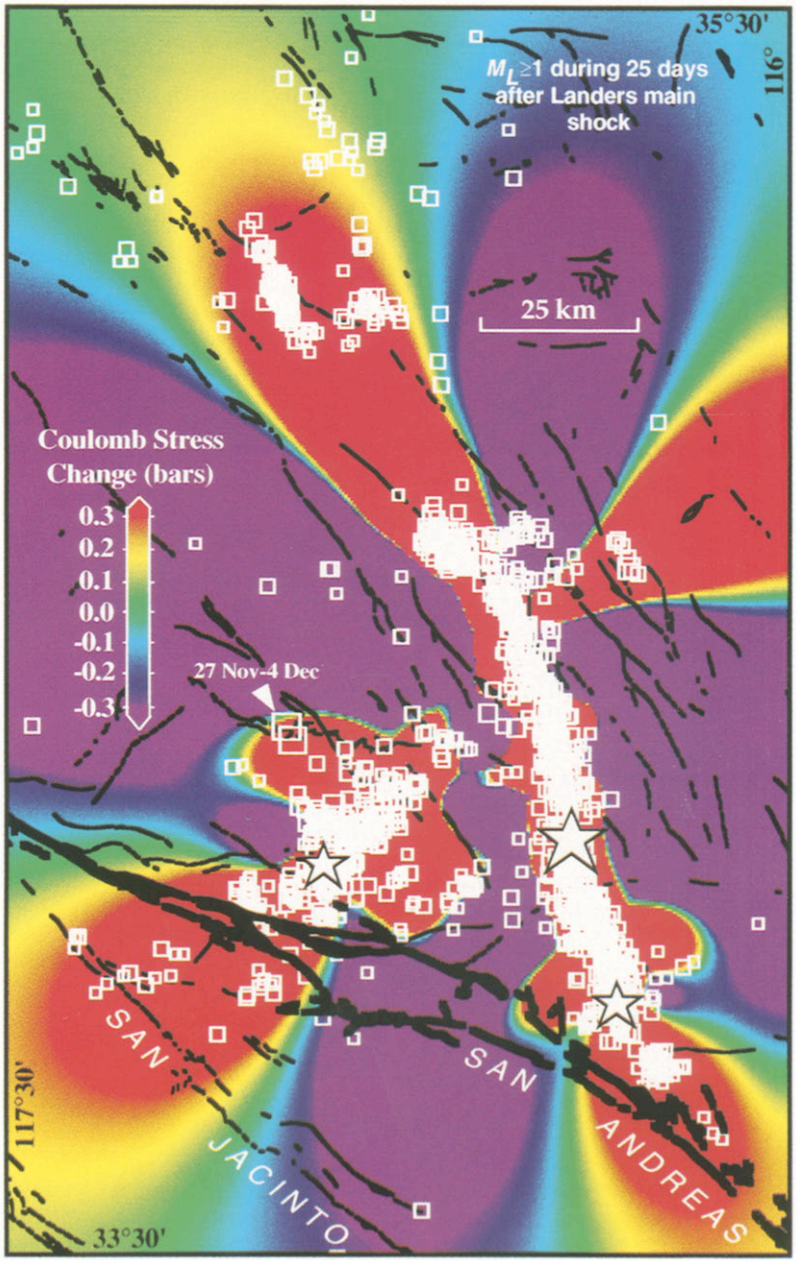

Figure 13. The largest Coulomb stress changes at depths between 0 and 12.5 km caused by the Landers, Big Bear, and Joshua Tree earthquakes, shown with the first 25 days of seismicity from Hauksson *et al.* (1993). Also shown are the largest two aftershocks to occur during the following 8 months, the 17 November 1992 M_L = 5.3 and 4 December 1992 M_L = 5.1 shocks.

tonic block surrounded by a stiffer crust, consistent with the *Pg* velocity contours of Hearn and Clayton (1986). The average velocity contrast between the 100- by 300-km Mojave region with *Pg* velocity <6.2 km/sec and the surrounding medium is 0.45 km/sec. We gave the Mojave block a Young's modulus, E, of 6.2×10^{11} dyne-cm^{-2}. In this plane stress calculation, the Coulomb failure stress rise is halved in the Coachella Valley, but is nearly unchanged elsewhere. Thus, although we may overestimate the stress change for the Coachella Valley in Figure 12, a stress increase did apparently occur, but has not been expressed in seismicity.

In Figure 13 we plot the most positive Coulomb stress change at depths between 0.5 and 12.5 km. Thus, this is the Coulomb stress change on optimally oriented faults at the optimum depth. This function gives perhaps the best correlation between stress changes and aftershocks, since aftershocks will likely occur at the depth and location where the stress change is greatest. Note that two of the largest earthquakes in southern California during the 9-month period, the 27 November 1992 $M_L = 5.3$ and the 4 December 1992 $M_L = 5.1$ events, occurred north of the Big Bear epicenter in a region where stress was increased as a result of the Big Bear earthquake.

Coulomb Stress Changes along the San Andreas and San Jacinto Faults

Thus far we have been calculating Coulomb stress changes on optimally oriented planes $\Delta\sigma_f^{\text{opt}}$. This is because for small events, sufficient small faults exist that those optimally orientated will be activated. The only possible exceptions have been the Landers and Big Bear earthquakes, but in both cases, the difference between optimum and actual orientations were small. The San Andreas and San Jacinto faults are not optimally orientated, so to examine Coulomb changes we resolve the right-lateral Coulomb stress changes on these faults $\Delta\sigma_f^R$, rather then calculate optimum changes at the fault locations $\Delta\sigma_f^{\text{opt}}$.

Resolved Coulomb changes for the San Andreas are shown in Figure 14. Because the failure stress change on a particular fault is independent of the regional stress, as illustrated in Figure 2a, the calculation is a function only of the Landers source and the San Andreas fault geometry, sense of slip, and friction coefficient. In the *top panel* of Figure 14, Coulomb stress changes are shown for $\mu = 0$ and $\mu = 0.75$. San Andreas segment boundaries inferred by the Working Group on California Earthquake Probabilities (1988) are shown below and accord roughly to sign changes in the failure stress change imposed by the Landers event. Regardless of the value of friction, the stress change is positive along the San Bernardino Mountain segment, generally positive along the Coachella Valley segment, and negative along the Mojave segment. The failure stress changes are greatest for high values of effective friction, reflecting the role that the normal stress plays in the total Coulomb stress change. The stress changes for an intermediate value of friction ($\mu = 0.4$) are shown in Figure 14 (*middle panel*). The stress change on the northern San Jacinto fault, which is farther from Landers but more favorably oriented than the San Andreas, is positive along parts of the San Bernardino Valley and San Jacinto Valley segments (Fig. 15, *upper panel*). These results are in substantial agreement with those of Harris and Simpson (1992) and Jaumé and Sykes (1992).

Potential Slip on the San Andreas and San Jacinto Faults Caused by the Landers Rupture

The correspondence between seismicity and the Coulomb failure stress changes produced by the Landers and earlier events suggests that regions of predicted increase are candidates for future major events. If the earthquakes are in some sense time-predictable, with rupture occurring when a failure threshold is exceeded, then the stress increase will hasten the time to the next earthquake. To predict how the Landers earthquakes have advanced or delayed the next great southern San Andreas earthquake, we let a frictionless San Andreas (Fig. 14, *bottom panel*) or San Jacinto fault (Fig. 15, *bottom panel*) slip to relieve the stress imposed by the Landers, Big Bear, and Joshua Tree earthquakes. This is accomplished by introducing freely slipping boundary elements along the faults to a depth of 12.5 km.

The response on the San Andreas is slip of 20 cm along the central San Bernardino segment (equivalent to an **M** = 6.2 event if it occurred seismically), and 7 cm in the northern Coachella Valley segment (equivalent to **M** = 5.7). The calculated slip does not depend on the number of San Andreas segments allowed to slip at once, or on the coefficient of friction. Slip on the San Andreas fault with a moment equivalent to two moderate events are therefore needed simply to relieve the stresses added by the Landers sequence. In contrast, potential slip comparable to an **M** = 6.2 event is removed from the Mojave segment, and slip equivalent to an **M** = 6 event is removed north of Palm Springs [site of the 1948 **M** = 6 Desert Hot Spring earthquake; see Sykes and Seeber (1985)], taking these portions of the fault farther from failure. On the San Jacinto fault, the San Bernardino Valley and San Jacinto Valley segments have an added potential for slip of 5 cm along the northernmost 50 km of the fault (Fig. 15, *lower panel*). So far creep has not been detected and no **M** > 5 earthquakes have occurred on the San Andreas or San Jacinto faults since the Landers event. If these events do not take place, the likelihood of great earthquakes on the San Andreas must increase as well.

Time Change to the next Large Earthquakes on the San Andreas and San Jacinto Faults

Because the southern San Andreas fault is late in the earthquake cycle, the long-term probability of a great earthquake on any of its three southern segments was high before the Landers earthquake took place (Working Group on California Earthquake Probabilities, 1988). The San Bernardino Mountain segment last ruptured in 1812 (Fumal *et al.*, 1993); given its 24 ± 3 mm/yr slip rate (Weldon and Sieh, 1985), a ≥4.3-m slip deficit has since accumulated, which could yield an **M** ≥ 7.5 event. The Coachella Valley segment last ruptured in 1680, has a

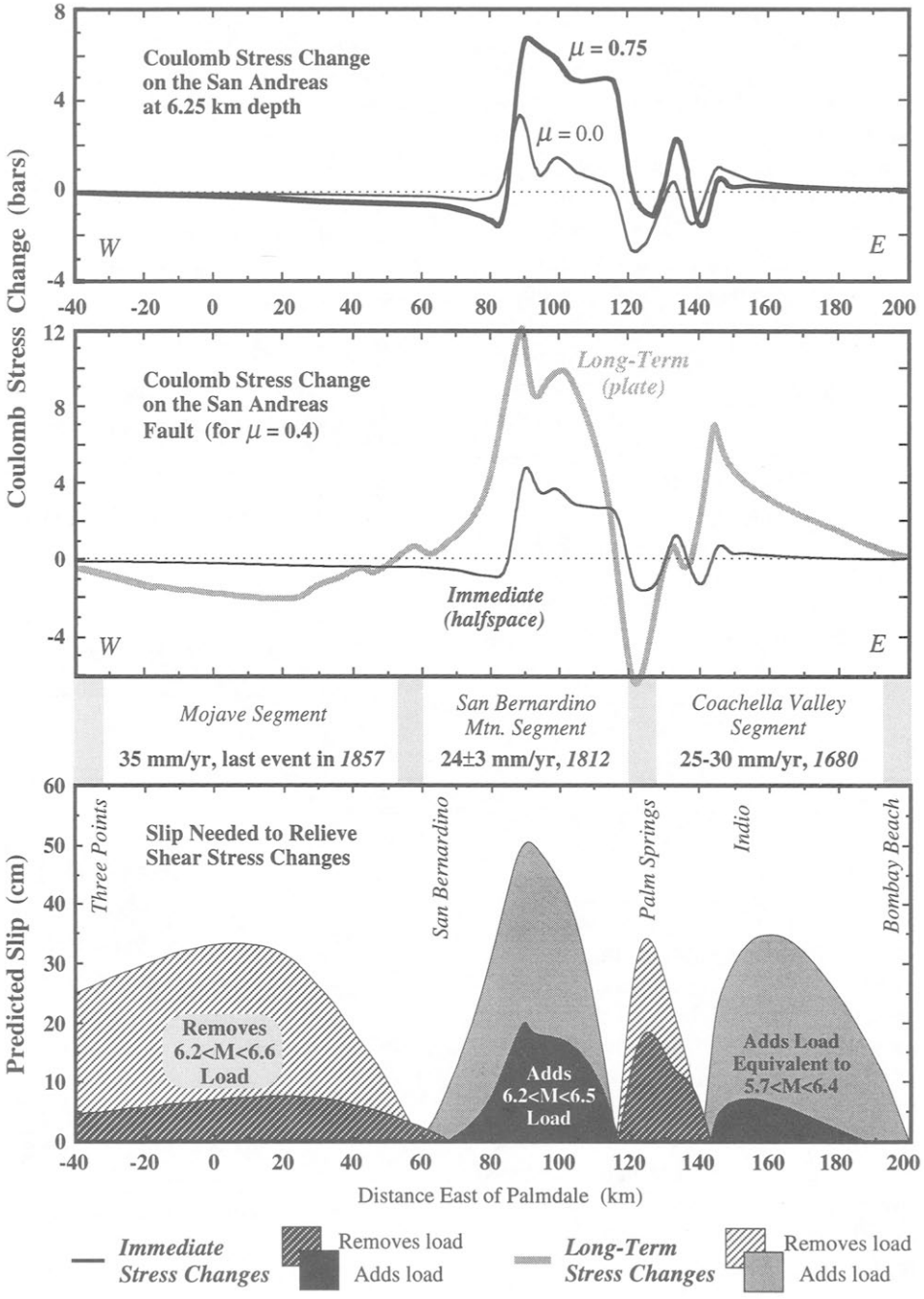

Figure 14. Coulomb stress change caused by the Landers, Big Bear, and Joshua Tree earthquakes resolved on the San Andreas fault (*top two panels*). The San Andreas is assumed to be vertical, purely right-lateral, and 12.5-km deep. The fault is traced along the Mission Creek branch (the northern strand between San Bernardino and Indio in Fig. 13) and stress is sampled every 5 km along the fault at a depth of 6.25 km. The *bottom panel* depicts the slip required to relieve the imposed stress increase.

slip rate of 25 to 30 mm/yr, and thus has accumulated a ≥ 6-m deficit (**M** ≥ 7.5). Its prehistoric repeat time is ≥235 yr (Lindh, 1988). The Mojave segment last ruptured in 1857, has a slip rate of ~35 mm/yr (Weldon and Sieh, 1985), and thus has accumulated a 4.7-m deficit (**M** ≥ 7.7); its repeat time is 100 to 130 yr (Fumal *et al.*, 1993; Jacoby *et al.*, 1988). The San Bernardino Valley segment of the San Jacinto fault may have last ruptured in 1890; it has a slip rate of 8 ± 3 mm/yr (Working Group on California Earthquake Probabilities, 1988), and thus has a slip deficit of ≥0.8 m (**M** ≥ 6.8).

We estimate the advance and delay times of great earthquakes by dividing the slip required to relieve the applied stress by the local San Andreas or San Jacinto slip rates. Alternatively, one could divide the calculated Coulomb or shear stress change by the assumed stress drop $\Delta\tau$ of the last earthquake, and then multiply this ratio by the next earthquake repeat time. Our calculation, however, benefits from being independent of the earthquake repeat time or earthquake stress drop, for which there is both uncertainty and variability. Our estimate probably supplies a lower bound on the earthquake time change because we neglect changes in normal stress acting on the fault, which tended to increase the Coulomb stress changes on the San Andreas.

We thus find that the next great San Andreas earthquake along the San Bernardino Mountain segment will strike 8 to 10 yr sooner than it would have in the absence of the Landers shock. Similarly, the next great San Andreas earthquake along the Coachella Valley segment is advanced by 2 yr; and the next large earthquake on the San Bernardino Valley segment of the San Jacinto fault is advanced 8 yr. In contrast, we estimate a delay in the next great Mojave shock by 2 yr.

Long-Term Stress Changes Caused by the Landers Earthquake Sequence

All of the calculations so far have been carried out in an elastic half-space on the assumption that for short periods of time, creep processes at depth can be ignored. Results from measuring and modeling earthquake-related geodetic data suggest that over periods of months to a year or two this is a reasonable approximation. However, stresses at depth will in due course relax and modify the stress distributions that we calculate. For example, after relaxation of the viscous substrate, the stress concentration below the fault shown in Figure 7 is transferred back to the elastic part of the crust. Relaxation of the lower crust reloads the upper crust, regardless of whether relaxation takes place by creep on the down-dip continuation of the fault, or by viscous flow in the lower crust or asthenosphere (Thatcher, 1990). We can therefore approximate complete relaxation of the lower crust by considering a 12.5-km-thick elastic plate over an inviscid fluid, with the material below the plate transmitting only vertical buoyancy forces to the plate. At the depths shown in our figures, the stress change on the San Andreas and surrounding faults roughly doubles (Fig. 14, *middle panel*, and Fig. 15, *upper panel*) and the slip required to relieve the stresses likewise grows (Fig. 14, *lower panel*, and Fig. 15, *lower panel*). The time needed for substantial relaxation depends on the viscosity of the lower crust, or on the rate at which creep propagates down the fault, which is perhaps in the range of 30 to 100 yr. Thus, the stress changes caused by major events such as Landers do not diminish with time; rather they grow and diffuse outward from the source. If one were also to include the secular rate of stressing caused by the

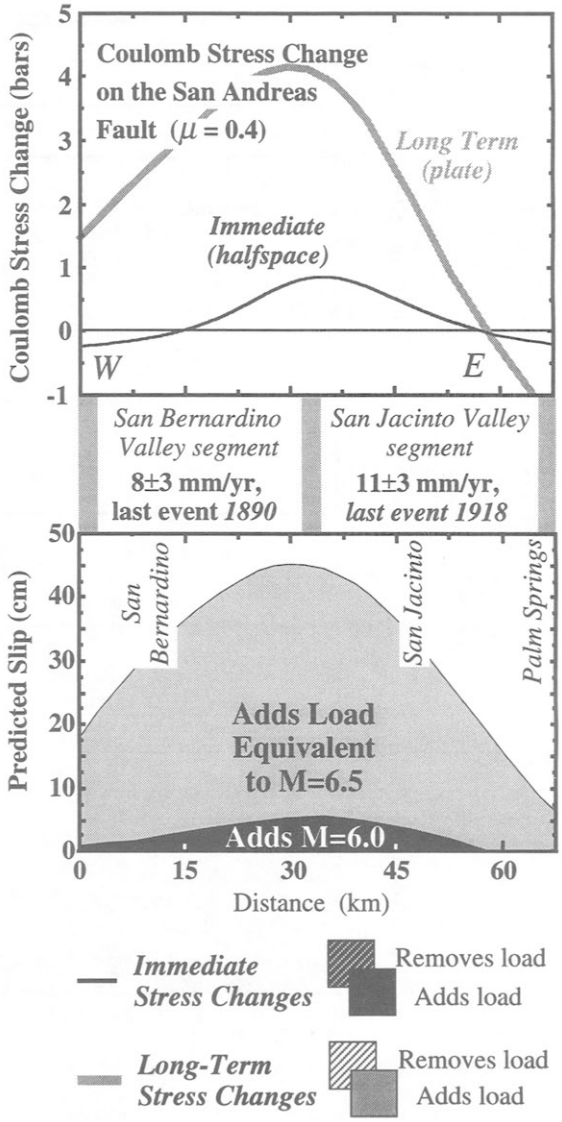

Figure 15. Coulomb stress change caused by the Landers, Big Bear, and Joshua Tree earthquakes resolved on the San Jacinto fault. The San Jacinto is assumed to be vertical, right-lateral, and 12.5-km deep; stress is sampled every 5 km along the fault at a depth of 6.25 km. The *lower panel* depicts the slip required to relieve the imposed stress increase.

plate tractions, the long-term stress changes would be larger still.

Conclusions

Earthquake slip causes stresses to change. The stress increases result in further earthquakes. Aftershocks are the most readily studied of such events because of their large number. The aftershocks of the Joshua Tree, Homestead Valley, Big Bear, and Landers earthquakes all have epicenter distributions that may be predicted on the basis of the Coulomb failure criterion; events occur where Coulomb stresses have risen. In the case of Joshua Tree and Homestead Valley, where the depth distributions of aftershocks are reliably determined, these are also effectively predicted by increases in Coulomb stresses. The exact locations of off-fault stress changes are modestly sensitive to assumptions about regional stress direction and, to a lesser extent, the effective friction coefficient. Since a range of plausible values can reproduce observed aftershock distributions, neither the effective friction coefficient nor the regional stress field is constrained by our results. Conversely, the predictive power of the method that we use does not depend on having a detailed knowledge of these parameters.

Stress increases of less than one-half bar appear sufficient to trigger earthquakes, and stress decreases of a similar amount are sufficient to suppress them. The former, in agreement with current ideas of self-organized criticality, suggests that some parts of the brittle crust are always on the threshold of failure. This indicates that over periods of aftershock sequences, other processes do not change stresses by even modest amounts.

Over long time periods Coulomb stress changes in the upper crust will increase as a result of stress relaxation processes in the lower crust. Thus, our calculations may understate the amplitude of the triggering stress for delayed events. Jaumé and Sykes (1992) and Simpson and Reasenberg (1994) have also argued that postseismic fluid flow will, under some circumstances, raise the effective coefficient of friction, causing long-term increases in the static stress changes. The time constant for these effects is subject to speculation, and thus we leave the evolution of the Coulomb stress changes to further study.

Coulomb stress changes do not only predict aftershock distributions. The Landers earthquake rupture occurred within a narrow zone where a series of previous events had enhanced Coulomb stresses. The Big Bear earthquake that followed Landers was also apparently controlled both in its initiation point (near the maximum Coulomb stress increase due to the Landers rupture) and in its termination point (where the Coulomb stress change was negative) by stresses due to the main event. These observations suggest that regions of enhanced Coulomb stress should be regarded as candidates for future events. The stresses transmitted by the Landers sequence to the nearby San Bernardino segment of the San Andreas fault are substantial, between 2 and 6 bars, and these could grow to 10 bars as the lower crust beneath Landers relaxes. The rate of small earthquakes has risen on this portion of the San Andreas since the Landers earthquake. But unless these stresses are relieved by the occurrence of an $M \sim 6.5$ event on the San Andreas, the next great earthquake on the San Bernardino segment may be advanced by a decade or more.

Acknowledgments

We are grateful for illuminating discussions with Albert Tarantola, Paul Tapponnier, and Ruth Harris. We thank Robert Simpson for conducting an extensive joint calibration of our respective programs. The calculations we report were carried out using the boundary element program VARC 0.9, written by King. The program incorporates half-space code modified from Okada (1992), and employs the methods outlined by Crouch and Starfield (1983) as modified by Bilham and King (1989) for freely slipping fault elements.

References

Ambraseys, N. N. (1970). Some characteristic features of the Anatolian fault zone, *Tectonophysics* **9**, 143–165.

Ammon, C. J., A. A. Velasco, and T. Lay (1993). Rapid estimation of rupture directivity: application to the 1992 Landers (M_S = 7.4) and Cape Mendocino (M_S = 7.2), California earthquakes, *Geophys. Res. Lett.* **20**, 97–100.

Bak, P. and C. Tang (1989). Earthquakes as self-organized critical phenomena, *J. Geophys. Res.* **94**, 15635–15637.

Bilham, R. G. and G. C. P. King (1989). The morphology of strike-slip faults—examples from the San Andreas fault, California, *J. Geophys. Res.* **94**, 10204–10216.

Cohee, B. P. and G. C. Beroza (1994). Slip distribution of the 1992 Landers earthquake and its implications for earthquake source mechanics, *Bull. Seism. Soc. Am.* **84**, no. 3.

Cowie, P. A., C. Vanneste, and D. Sornette (1993). Statistical physics model for the spatio-temporal evolution of faults, *J. Geophys. Res.* **98**, 21809–21821.

Crouch, S. L. and A. M. Starfield (1983). *Boundary Element Methods in Solid Mechanics*, Allen Unwin, London.

Das, S. and C. H. Scholz (1983). Off-fault aftershock clusters caused by shear stress increase? *Bull. Seism. Soc. Am.* **71**, 1669–1675.

DeMets, C., R. G. Gordon, D. F. Argus, and S. Stein (1990). Current plate motions, *Geophys. J. Int.* **101**, 425–478.

Fumal, T. E., S. K. Pezzopane, R. J. Weldon, II, and D. P. Schwartz (1993). A 100-year average recurrence interval for the San Andreas fault at Wrightwood, California, *Science* **259**, 199–203.

Hanks, T. C. and C. R. Allen (1989). The Elmore Ranch and Superstition Hills earthquakes of 24 November 1987: introduction to the special issue, *Bull. Seism. Soc. Am.* **79**, 231–237.

Harris, R. A. and R. W. Simpson (1992). Changes in static stress on southern California faults after the 1992 Landers earthquake, *Nature* **360**, 251–254.

Hauksson, E., L. M. Jones, K. Hutton, and D. Eberhart-Phillips (1993). The 1992 Landers earthquake sequence: seismological observations, *J. Geophys. Res.* **98**, 19835–19858.

Hearn, T. M. and R. W. Clayton (1986). Lateral variations in southern California, I. Results for the upper crust from *Pg* waves, *Bull. Seism. Soc. Am.* **76**, 495–509.

Hecker, S., T. E. Fumal, T. J. Powers, J. C. Hamilton, C. D. Gar-

vin, and D. P. Schwartz (1993). Late Pleistocene-Holocene behavior of the Homestead valley fault segment—1992 Landers, Ca surface rupture, *EOS Supplement*, 1993 Fall Meeting, 612.

Hill, D. P., P. A. Reasenberg, A. Michael, W. J. Arabaz, G. Beroza, D. Brumbaugh, J. N. Brune, R. Castro, S. Davis, D. dePolo, W. L. Ellsworth, J. Gomberg, S. Harmsen, L. House, S. M. Jackson, M. J. S. Johnston, L. Jones, R. Keller, S. Malone, L. Munguia, S. Nava, J. C. Pechmann, A. Sanford, R. W. Simpson, R. B. Smith, M. Stark, M. Stickney, A. Vidal, A. Walter, V. Wong, and J. Zollweg (1993). Seismicity remotely triggered by the magnitude 7.3 Landers, California, earthquake, *Science* **260**, 1617–1623.

Hill, R. L. and D. J. Beeby (1977). Surface faulting associated with the 5.2 magnitude Galway Lake earthquake of May 31, 1975: Mojave Desert, San Bernardino County, California, *Geol. Soc. Am. Bull.* **88**, 1378–1384.

Hudnut, K. W., L. Seeber, and J. Pacheco (1989). Cross-fault triggering in the November 1987 Superstition Hills earthquake sequence, southern California, *Geophys. Res. Lett.* **16**, 199–202.

Hutton, L. K., C. E. Johnson, J. C. Pechmann, J. E. Ebel, T. W. Given, D. M. Cole, and P. T. German (1980). Epicentral locations for the Homestead Valley earthquake sequence, March 15, 1979, *Calif. Geol.* **33**, 110–116.

Jacoby, G. C., K. E. Sieh, and P. R. Shepard (1988). Irregular recurrence of large earthquakes along the San Andreas fault—evidence from trees, *Science* **241**, 196–199.

Jaeger, J. C. and N. G. W. Cook (1979). *Fundamentals of Rock Mechanics*, 3rd ed., Chapman and Hall, London.

Jaumé, S. C. and L. R. Sykes (1992). Change in the state of stress on the southern San Andreas fault resulting from the California earthquake sequence of April to June 1992, *Science* **258**, 1325–1328.

Jones, L. E. and S. E. Hough (1994). Analysis of broadband records from the June 28, 1992 Big Bear earthquake: evidence of a multiple-event source, *Bull. Seism. Soc. Am.* **84**, no. 3.

Jones, L. M. (1988). Focal mechanisms and the state of stress on the San Andreas fault in southern California, *J. Geophys. Res.* **93**, 8869–8891.

Jones, L. M., K. Hutton, D. A. Given, and C. R. Allen (1986). The July 1986 North Palm Springs, California, earthquake, *Bull. Seism. Soc. Am.* **76**, 1830–1837.

King, N. E., D. C. Agnew, and F. Wyatt (1988). Comparing strain events: a case study for the Homestead Valley earthquakes, *Bull. Seism. Soc. Am.* **78**, 1693–1706.

Larsen, S., R. Reilinger, H. Neugebauer, and W. Strange (1992). Global Positioning System measurements of deformations associated with the 1987 Superstition Hills earthquake: evidence of conjugate faulting, *J. Geophys. Res.* **97**, 4885–4902.

Lindh, A., G. Fuis, and C. Mantis (1978). Seismic amplitude measurements suggest foreshocks have different focal mechanisms than aftershocks, *Science* **201**, 56–59.

Lindh, A. G. (1988). Estimates of long-term probabilities for large earthquakes along selected fault segments of the San Andreas fault system in California, in *Earthquake Prediction: Present Status*, S. K. Guha and A. M. Patwardhan (Editors) University of Poona, Pune, India, 189–200.

Lisowski, M., J. C. Savage, and W. H. Prescott (1991). The velocity field along the San Andreas fault in central and southern California, *J. Geophys. Res.* **96**, 8369–8389.

Massonnet, D., M. Rossi, C. Carmona, F. Adranga, G. Peltzer, K. Feigl, and T. Rabaute (1993). The displacement field of the Landers earthquake mapped by radar interferometry, *Nature* **364**, 138–142.

Murray, M. H., J. C. Savage, M. Lisowski, and W. K. Gross (1993). Coseismic displacements: 1992 Landers, California, earthquake, *Geophys. Res. Lett.* **20**, 623–626.

Nur, A., H. Ron, and G. C. Beroza, (1993). The nature of the Landers-Mojave earthquake line, *Science* **261**, 201–203.

Okada, Y. (1992). Internal deformation due to shear and tensile faults in a half-space, *Bull. Seism. Soc. Am.* **82**, 1018–1040.

Oppenheimer, D. H., P. A. Reasenberg, and R. W. Simpson (1988). Fault plane solutions for the 1984 Morgan Hill, California, earthquake sequence: evidence for the state of stress on the Calaveras fault, *J. Geophys. Res.* **93**, 9007–9026.

Pacheco, J. and J. Nábelek (1988). Source mechanisms of three moderate California earthquakes of July 1986, *Bull. Seism. Soc. Am.* **78**, 1907–1929.

Reasenberg, P. A. and R. W. Simpson (1992). Response of regional seismicity to the static stress change produced by the Loma Prieta earthquake, *Science* **255**, 1687–1690.

Rockwell, T. K., D. P. Schwartz, K. Sieh, C. Rubin, S. Lindvall, M. Herzberg, D. Padgett, and T. Fumal (1993). Initial Paleoseismic studies following the Landers earthquake: implications for fault segmentation and earthquake clustering, *EOS Supplement*, 1993 Fall Meeting, 67.

Rubin, C. and K. Sieh (1993). Long recurrence interval for the Emerson fault: implications for slip rates and probabilistic seismic hazard calculations, *EOS Supplement*, 1993 Fall Meeting, 612.

Sanders, C. O. (1993). Interaction of the San Jacinto and San Andreas fault zones, southern California: triggered earthquake migration and coupled recurrence intervals, *Science* **260**, 973–976.

Sauber, J., W. Thatcher, and S. C. Solomon (1986). Geodetic measurement of deformation in the central Mojave Desert, California, *J. Geophys. Res.* **91**, 12683–12693.

Savage, J. C., M. Lisowski, and M. Murray (1993). Deformation from 1973 to 1991 in the epicentral area of the 1992 Landers, California, earthquake (M_S = 7.5), *J. Geophys. Res.* **98**, 19951–19958.

Scholz, C. H. (1982). Scaling laws for large earthquakes: consequences for physical models, *Bull. Seism. Soc. Am.* **72**, 1–14.

Shamir, G. and M. D. Zoback (1992). Stress orientation profile to 3.5 km depth near the San Andreas fault at Cajon Pass, California, *J. Geophys. Res.* **97**, 5059–5080.

Sieh, K., L. Jones, E. Hauksson, K. Hudnut, D. Eberhart-Phillips, T. Heaton, S. Hough, K. Hutton, H. Kanamori, A. Lilje, S. Lindvall, S. F. McGill, J. Mori, C. Rubin, J. A. Spotila, J. Stock, H. K. Thio, J. Treiman, B. Wernicke, and J. Zachariasen (1993). Near-field investigations of the Landers earthquake sequence, April to July 1992, *Science* **260**, 171–176.

Simpson, R. W. and P. A. Reasenberg (1994). Earthquake-induced static stress changes on central California faults, in *The Loma Prieta, California, earthquake of October 17, 1989—techtonic processes and models*, R. W. Simpson (Editor), *U.S. Geol. Surv. Profess. Pap. 1550-F*.

Stein, R. S., G. C. P. King, and J. Lin (1992). Change in failure stress on the southern San Andreas fault system caused by the 1992 magnitude = 7.4 Landers earthquake, *Science* **258**, 1328–1332.

Stein, R. S. and M. Lisowski (1983). The 1979 Homestead Valley earthquake sequence, California: control of aftershocks and postseismic deformation, *J. Geophys. Res.* **88**, 6477–6490.

Sykes, L. R. and L. Seeber (1985). Great earthquakes and great asperities, San Andreas fault, southern California, *Geology* **13**, 835–838.

Thatcher, W. (1990). Present-day crustal movements and the mechanics of cyclic deformation, in *The San Andreas Fault System, California*, R. E. Wallace (Editor), *U.S. Geol. Surv. Profess. Pap. 1515*, 189–206.

Wald, D. J. and T. H. Heaton (1994). Spatial and temporal distribution of slip for the 1992 Landers, California earthquake, *Bull. Seism. Soc. Am.* **84**, no. 3.

Weldon, R. J., II and K. E. Sieh (1985). Holocene rate of slip and tentative recurrence interval for large earthquakes on the San An-

dreas fault in Cajon Pass, southern California, *Geol. Soc. Am. Bull.* **96**, 793–812.

Williams, P. L., L. R. Sykes, C. Nicholson, and L. Seeber (1990). Seismotectonics of the easternmost Transverse Ranges, California: relevance for seismic potential of the southern San Andreas fault, *Tectonics* **9**, 185–204.

Working Group on California Earthquake Probabilities (1988). Probabilities of large earthquakes occurring in California on the San Andreas fault, *U.S. Geol. Surv. Open-File Rept. 88-398*, 1–62.

Zoback, M. D. and A. H. Lachenbruch (1992). Introduction to special section on the Cajon Pass scientific drilling project, *J. Geophys. Res.* **97**, 4991–4994.

Institut de Physique du Globe
67084 Strasbourg France
(G.C.P.K.)

U.S. Geological Survey
Menlo Park, California 94025
(R.S.S.)

Woods Hole Oceanographic Institution
Woods Hole, Massachusetts 02543
(J.L.)

Manuscript received 20 August 1993.